Journal of Alloys and Compounds 509 (2011) 1124–1128

Contents lists available at ScienceDirect

Journal of Alloys and Compounds

journal homepage: www.elsevier.com/locate/jallcom

Fe–Al phase formation around SHS reactions under isothermal conditions

Ewelina Pocheć*, Stanisław Jóźwiak, Krzysztof Karczewski, Zbigniew Bojar

Department of Advanced Materials and Technology, Military University of Technology Kaliskiego 2 St., 00-908 Warsaw, Poland

ARTICLE INFO

Article history:
Received 19 May 2010
Received in revised form 10 August 2010
Accepted 18 August 2010
Available online 27 August 2010

Keywords:
Intermetallics
Sintering
Scanning electron microscopy (SEM)
X-ray diffraction
Phase transitions

ABSTRACT

This study investigates the phenomena preceding and accompanying the SHS reaction between Fe and Al elemental powders during sintering. SEM and XRD analysis were used to observe the mechanisms of formation of Fe–Al intermetallic phases. The analysis of sintered material just before the SHS reaction demonstrates that in addition to the well-known Fe_2Al_5 phase and the low-aluminum solid solution of iron, the high-aluminum phases $FeAl_2$ and $FeAl_3$ are formed. The kinetics of phase transformations under isothermal conditions were investigated by DSC using the JMA (Johnson–Mehl–Avrami) model. This approach allowed us to calculate Avrami coefficients, which characterize the speed and the manner of particular phase transformations.

1. Introduction

The process of formation of Fe–Al phases has been a subject of interest for many years and has been extensively studied. Many different theories have been developed to explain the mechanisms occurring during phase formation. One of the main theories was developed by Gedevanishvili and Deevi [1], who observed that two exothermic reactions occur during the heating of a mixture of Fe and Al powders. In the temperature range of 540–560 °C, self-propagating high-temperature synthesis (SHS) [2,6,7,8] occurs and is responsible for the formation of the hard and fragile Fe_2Al_5 phase. The next reaction, in the temperature range of 650–670 °C, leads to the nucleation and growth of a secondary FeAl solid solution. This second reaction results from the interaction between the remaining iron and the Fe_2Al_5 phase, as confirmed by Gao et al. [3]. Wei-Jen and Wang coated mild steel by hot-dipping in a molten aluminum bath, and they obtained thin layers of $FeAl_3$ and Fe_2Al_5 phases) [4]. Other authors have observed a more extensive set of Fe–Al phases ($FeAl_3$, $FeAl_2$, Fe_2Al_5, Fe_3Al and FeAl) after sintering and SHS reaction [5,10]

The aim of this paper is to explain the phenomena that occur before and during the SHS reaction. It is very important to understand the phase transformations that occur around the SHS reaction because they can influence the final structure of Fe–Al sinters. The results obtained in this study show that prior to the SHS reaction, the sinter structure contains not only the high-aluminum Fe_2Al_5 phase and the low-aluminum Fe(Al) solid solution but also the high-aluminum $FeAl_2$ and $FeAl_3$ phases.

2. Experimental (materials and methods, theory and calculation)

Elemental powders of 99.8% pure iron with an average particle size of 200 μm and 99.6% pure aluminum with an average particle size of 70 μm were mixed at a stoichiometric ratio of 50 at.% Fe: 50 at.% Al in a Uniball 5 mill (without milling balls) for 1 h. Then, the cylindrical DSC specimens (3 mm in diameter and 20 mg in weight) were uniaxially cold compacted at a pressure of 700 MPa.

The structure and chemical composition of the resulting material were conducted using SEM (Philips XL30LaB$_6$) with EDS (EDAX-DX4). XRD (Seifert 3000) with Co radiation and the PDF-2 database was used to complete the phase analysis. Based on XRD patterns and the Bragg condition, the iron lattice parameter was determined at different annealing temperatures. According to Vegard's law (1), a linear relationship exists at constant temperature between the crystal lattice parameter of an alloy and the concentrations of the constituent elements.

$$a_r = a_1 + (a_2 - a_1)C/100 \quad (1)$$

where: a_r – solid solution lattice constant; a_1 – dissolvent lattice constant; a_2 – dissolved element lattice constant; C – content of dissolved element.

The aluminum content in Fe(Al) solid solution was also determined. XRD patterns and the Hall–Williamson method (2) were used to determine the dimension and degree of deformation of the Fe crystal lattice to determine the recovery and recrystallization temperatures.

$$B_c = \frac{K\lambda}{D_{hkl}\cos\theta_{hkl}} + 4tg\theta_{hkl}\frac{\Delta a}{a} \quad (2)$$

where: B_c – peak width; K – Scherrer constant; λ – wavelength; D_{hkl} – average of crystal dimension; θ_{hkl} – the angle between the incident ray and the scattering planes; a – lattice constant; Δa – lattice deformation.

The kinetics of phase transformations were determined using a Differential Scanning Calorimeter (Setaram Labsys DSC/DTA/TG) under isothermal conditions and over a temperature range of 570–630 °C.

To explain the phenomena that occur during the SHS reaction, the microhardness was measured. For this purpose, samples with a diameter of 10 mm and a

* Corresponding author. Tel.: +48 22 683 95 45; fax: +48 22 683 95 45.
E-mail address: epochec@wat.edu.pl (E. Pocheć).

0925-8388/$ – see front matter © 2010 Elsevier B.V. All rights reserved.
doi:10.1016/j.jallcom.2010.08.074

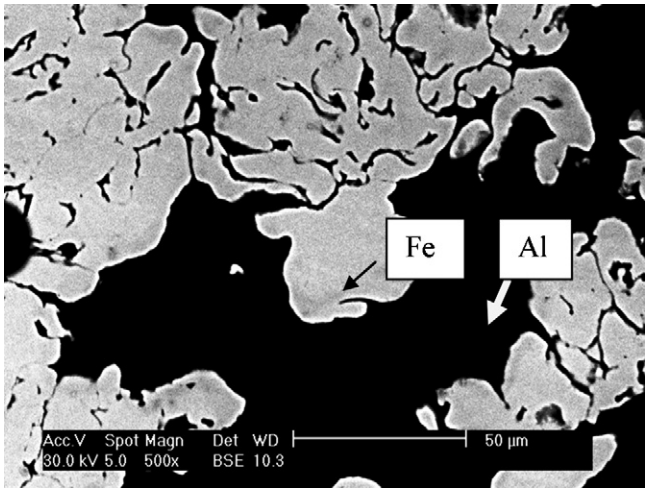

Fig. 1. A mixture of elemental Fe and Al powder particles after uniaxial compaction and isothermal sintering at 350 °C.

height of 5 mm were made by pressing at a pressure of 700 MPa and heating in the temperature range of 570–630 °C.

3. Results

SEM structural observations supported by EDS chemical microanalysis results indicate a strong influence of processing temperature on the phase composition of sinters. For low temperature sintering up to 300 °C, no effects are observed of diffusion at the points of contact between Fe and Al particles (Fig. 1). The precise control of the lattice parameter value based on XRD measurements (Fig. 2) shows that for temperatures up to about 600 °C, only a small amount of aluminum is dissolved in the alpha-iron crystal lattice. This low-aluminum Fe(Al) solid solution does not result in strengthening of the sintered material (Fig. 3). These effects are related to the recovery and recrystallization of iron in the range of 300–500 °C and aluminum in the range of 270–480 °C. Heat energy provided to the material leads to the recovery of iron in the temperature range of 300–400 °C (which is visible in changes in the degree of lattice deformation and in the increase in the iron crystal lattice dimension as seen in Fig. 3), and then the recrystallization of iron occurs in the temperature range of 400–500 °C. As a result, the speed of aluminum diffusion decreases and the aluminum content in the crystal lattice of iron slowly increases (zone 2 in Fig. 2).

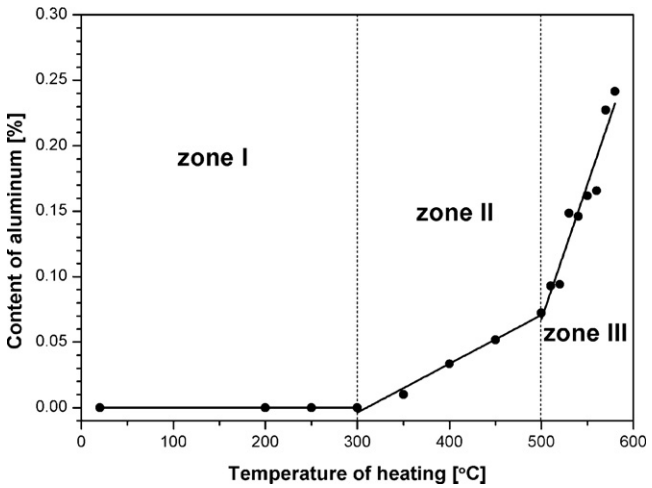

Fig. 2. Aluminum content in Fe_{α}-based solid solutions.

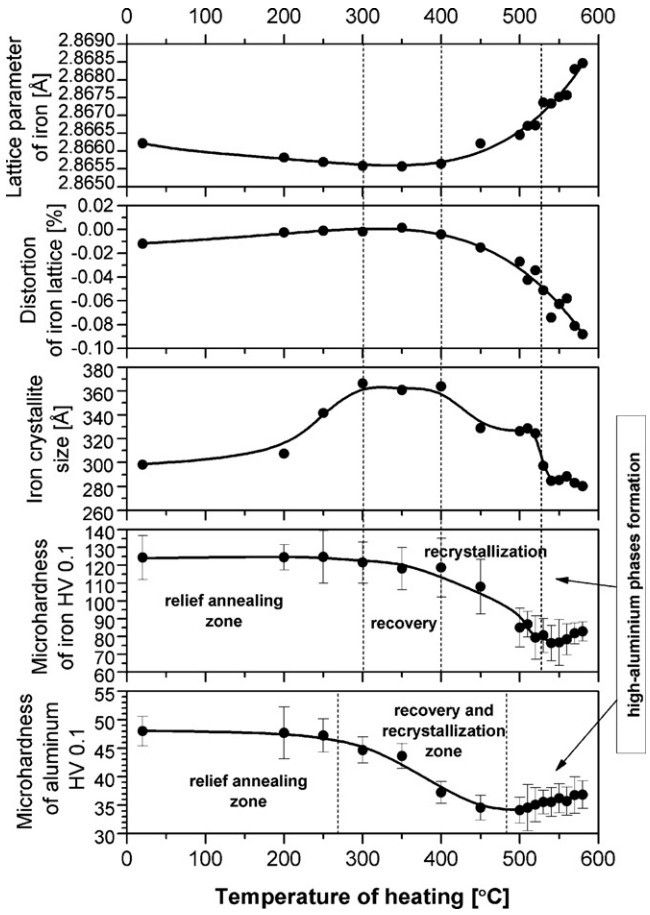

Fig. 3. Effects of isothermal heating temperature on various parameters.

After the thermally activated effects above 500 °C are complete, the aluminum content increases rapidly (zone 3 in Fig. 2). Further microhardness measurements show a slight increase at temperatures above 500 °C [9]. This increase in microhardness likely results

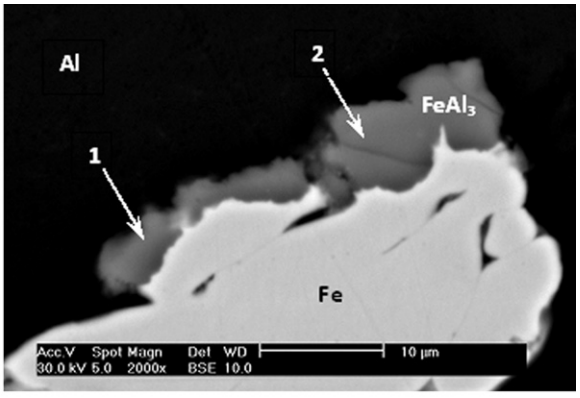

	1			2	
Element	Wt %	At %	Element	Wt %	At %
AlK	58,85	74,75	AlK	57,43	73,63
FeK	41,15	25,25	FeK	42,57	26,37
Total	100	100	Total	100	100

Fig. 4. $FeAl_3$ microzone at the region of contact between Fe and Al particles following isothermal sintering at 400 °C and the chemical composition in that region.

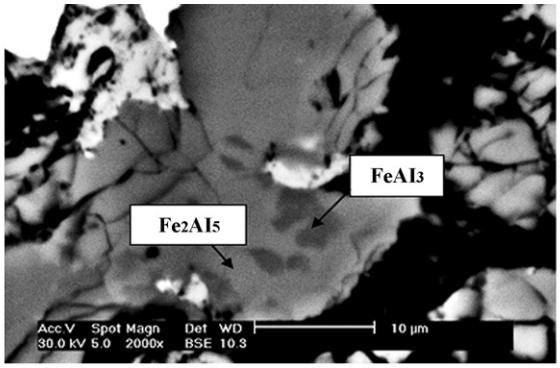

$FeAl_3$			Fe_2Al_5		
Element	Wt %	At %	Element	Wt %	At %
AlK	59,25	75,06	AlK	53,44	70,37
FeK	40,75	24,94	FeK	46,56	29,63
Total	100	100	Total	100	100

Fig. 5. BSE contrast between Fe_2Al_5 and $FeAl_3$ phases after isothermal sintering at 570 °C.

Table 1
Phase composition of sinters evaluated by DSC.

Heating temperature (°C)	$FeAl_3$	Fe_2Al_5	$FeAl_2$	FeAl
570–605	+	+	–	–
607–612	+	+	+	–
615–630	+	+	+	+

from the formation of $FeAl_3$ and then Fe_2Al_5 high-aluminum phase subareas. These areas are visible as a new $FeAl_3$ phase microzone as a result of diffusion at the contacts between Fe and Al particles after sintering in the temperature range of 400–500 °C (Fig. 4). Chemical composition analysis of the Al-rich precipitates demonstrates that increasing the sintering temperature increases the mass transport of iron and aluminum atoms and the volume of dark-grey aluminum-reach subareas as detected by BSE. As a result, at a temperature of 570 °C, in addition to aluminum and iron powder particles, high-aluminum phases such as $FeAl_3$ and Fe_2Al_5 are observed (Fig. 5). At this stage, no precipitates were observed from the B2-ordered FeAl secondary solid solution.

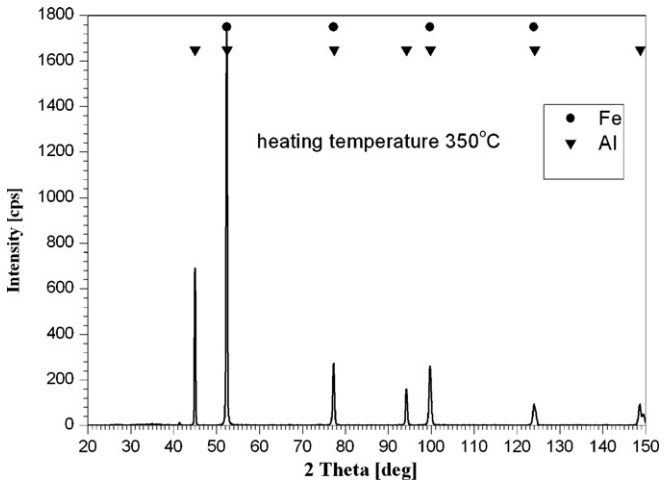

Fig. 6. XRD patterns with Al (A1 lattice) and Fe (A2 lattice) peaks noted for samples after isothermal sintering at 350 °C.

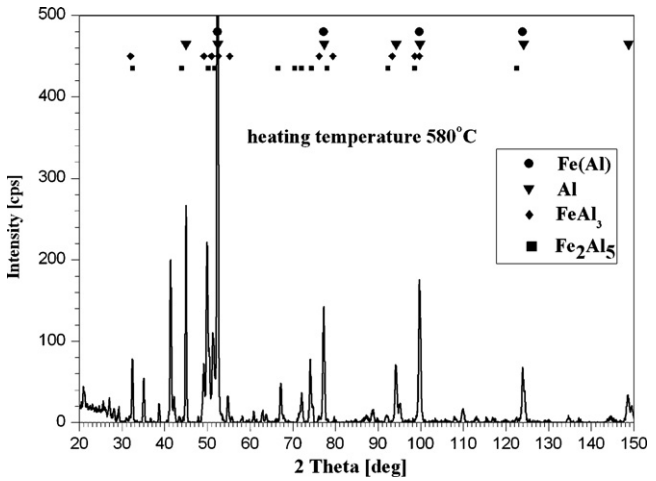

Fig. 7. Complex XRD pattern of an Fe–Al sample after isothermal sintering at 580 °C.

Table 2
The values of the Avrami exponent for all identified phases at given temperatures.

Avrami exponent				
T (°C]	$FeAl_3$	Fe_2Al_5	$FeAl_2$	FeAl
570	4.9	10.5	–	–
580	4.7	4.6	–	–
585	8.8	3.8	–	–
590	3.3	9.2	–	–
595	5.1	6.9	–	–
600	5.1	6.2	4.8	–
605	1.8	2.7	4.4	–
610	5.8	4.9	3	–
615	4.6	3.8	8.6	3.8
617	20.2	12.6	13	8.5
620	23.7	17.5	11.8	8.9
630	11.2	10.4	7.8	5.9

The above conclusions were confirmed by XRD analysis for the samples sintered under isothermal conditions (Fig. 6 and Fig. 7). XRD analysis of samples sintered at temperatures up to 350 °C shows peaks from only Fe_α and Al, whereas the material sintered at 580 °C exhibits peaks from high-aluminum $FeAl_3$ and Fe_2Al_5 phases.

Self-propagating high-temperature synthesis (SHS) occurred at sintering temperatures above 580 °C. SHS delivers considerable

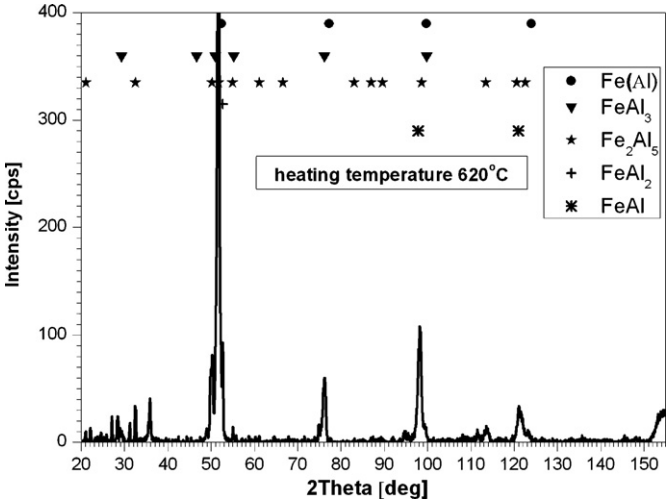

Fig. 8. XRD pattern after sintering at 620 °C.

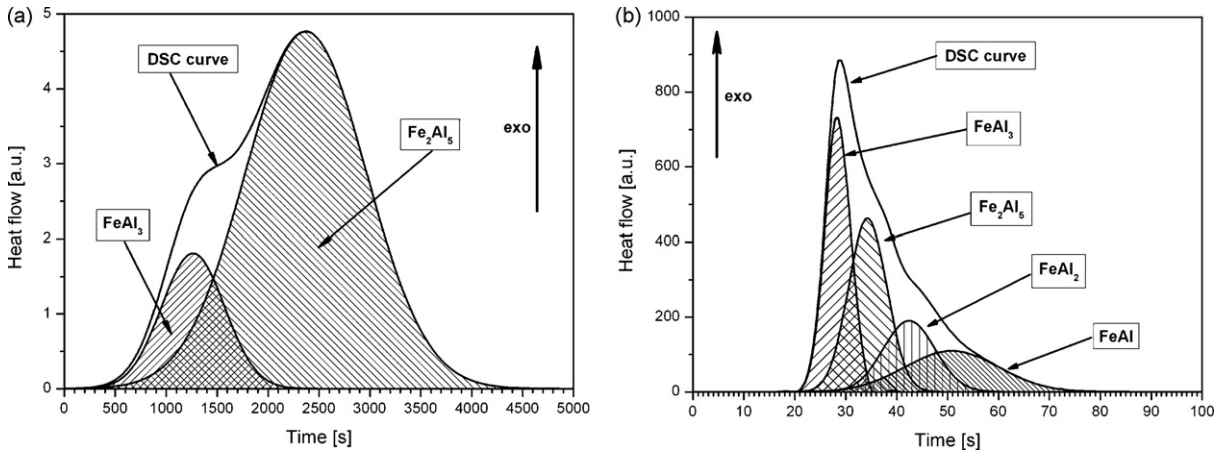

Fig. 9. DSC heat flow curve during isothermal annealing at 580 °C (a) and 630 °C (b) separated into peaks responsible for the creation of different Fe–Al phases.

energy, which leads to the appearance of an FeAl phase (Fig. 8). The rapid rate of the SHS reaction makes it impossible to observe by classical methods such as SEM and XRD. Therefore, DSC [11] and JMA modeling [11,12,13] were used to determine the basic kinetic parameters of the reaction including the Avrami exponent, which characterizes the speed and the manner of particular phase formations [16].

The complexity of isothermal solid state transformation phenomena can be described by the JMA equation [14,11]:

$$\alpha(t) = 1 - \exp[-(Kt)^n] \quad (3)$$

where $\alpha(t)$ is the degree of transformation and n is the Avrami exponent characterizing the speed and the manner of a particular phase transformation.

Taking the double logarithm of each side of Eq. (1), we obtain:

$$\ln[-\ln(1-\alpha(t))] = n\ln K + n\ln t \quad (4)$$

In analyzing the kinetics of phase transformations, it is highly useful to plot the quantity $[-\ln(1-\alpha(t))]$ versus time on a double-logarithmic plot. In this case, the slope of the straight line designates the Avrami exponent n.

The shape of the DSC curves and the XRD phase analysis results for samples sintered under different conditions reveal the different phases that appear at different temperatures. In turn, this allows the kinetic parameters of phase transformations to be determined. Taking into account the Fe–Al phase equilibrium diagram [15] and rules of diffusion mass transport, the sequence of phases appearing during sintering should be $FeAl_3 \rightarrow Fe_2Al_5 \rightarrow FeAl_2 \rightarrow FeAl$.

The heat flow effect observed by DSC, represented as the surface under the DSC curve in Fig. 9, consists of elemental heat streams from phases occurring in certain sintering conditions. The overall DSC curve can be divided into these elemental peaks using the JMA model. This analysis leads to the best-fit DSC curves (Fig. 9). The probability of nucleation and growth of various Fe–Al phases depends on the amount of energy at the sintering temperature, as seen in Table 1.

Applying the JMA model to the DSC curves enabled us to determine the degree of phase transformation over time for all identified phases at the studied temperatures. Finally, the kinetics of phase transformation during isothermal sintering of a mixture of Fe and Al elemental powder particles were described (Fig. 10)

According to Eq. (2), for all energy peaks fitted to the main DSC curve, Avrami exponent values were assigned to each Fe–Al phase during nucleation and growth in isothermal heating (Fig. 11, Table 2).

Table 2 demonstrates that the Avrami exponent values for the identified phases are not constant during the phase rebuilding process. The Avrami exponents for the $FeAl_3$ and Fe_2Al_5 phases observed by XRD analysis (Fig. 12, Table 2) are approximately five

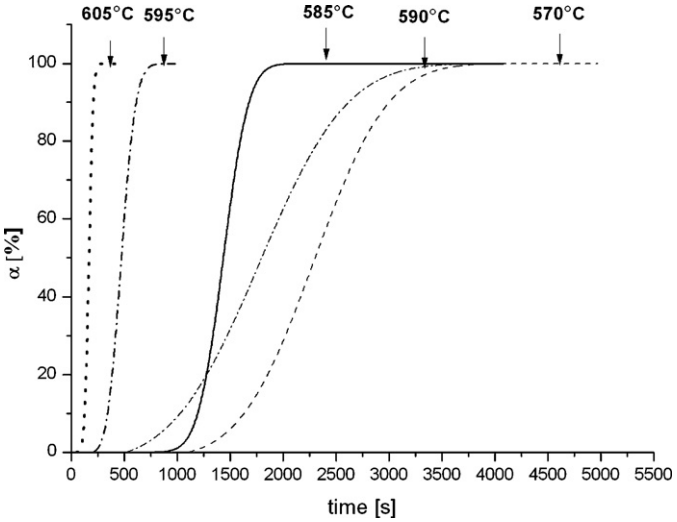

Fig. 10. Reaction kinetics for nucleation and growth of the $FeAl_3$ phase during isothermal sintering in the range of 570–605 °C.

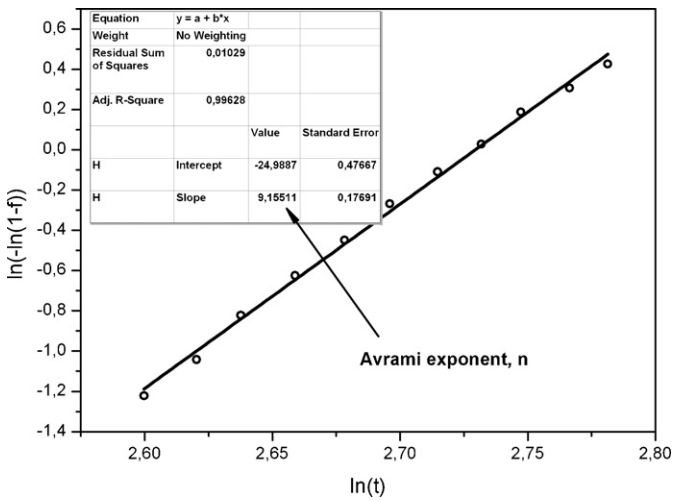

Fig. 11. The Avrami exponent n value determined as the slope of the ln(−ln(1-f) versus ln(t) curve for the sample sintered at 590 °C;($n = 9.2 \pm 0.18$).

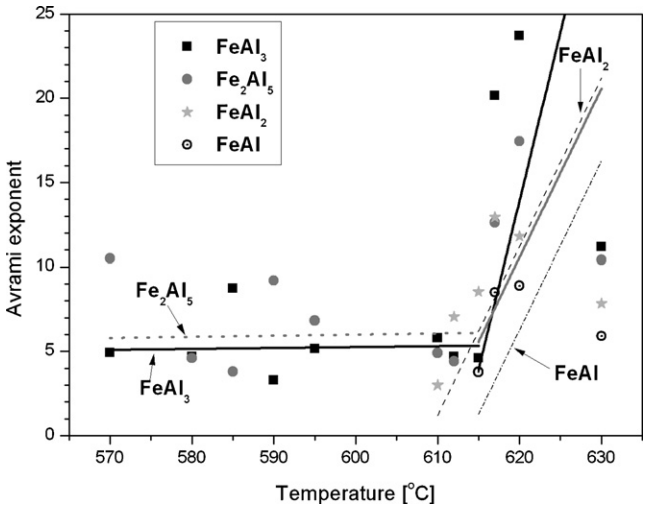

Fig. 12. Avrami exponent calculated for isothermal conditions.

at temperature ranges up to 615 °C. These Avrami exponent values prove the mainly diffusive nature of those phases [16]. Above 615 °C, the Avrami parameter grows significantly (Fig. 12), demonstrating a significant intensification of $FeAl_3$ and Fe_2Al_5 nucleation and growth in that temperature range. The SHS reaction initiated at that temperature seems to be responsible for this process as well for the formation of the $FeAl_2$ and FeAl phases.

4. Conclusions

This study examined the isothermal sintering of a mixture of Fe and Al elemental powders in the temperature range of 570–630 °C. SEM, DSC and XRD measurements confirmed the presence of the entire spectrum of Fe–Al phases in tested sinters. The results demonstrate that there are two mechanisms of formation of Fe–Al phases. First, high-aluminum $FeAl_3$ and Fe_2Al_5 phases form by slow diffusion-controlled formation at temperatures up to 615 °C. The second mechanism is related to the self-propagating high-temperature synthesis (SHS) initiated at approximately 615 °C. The SHS reaction provides a large amount of energy and allows for the creation of the high-aluminum fragile $FeAl_2$ phase and an FeAl ordered secondary solid solution. The secondary solid solution is expected to be the final phase and to occur in high amounts. No influence was observed of the Fe(Al) solid solution on the mechanism of FeAl phase formation. The FeAl phase can only be obtained as a final structure of intermetallic sinter after an additional homogenization process. These results confirm that the processing temperature is an important parameter for isothermal sintering.

Acknowledgements

This work was supported by the Polish Ministry of Science and Higher Education (Grant No. OR 00 0057 06, ON 508 004334 and 000 01104).

References

[1] S. Gedevanishvili, S.C. Deevi, Materials Science and Engineering A 325 (2002) 163–176.
[2] G. Merzhanov, Journal of Materials Processing Technology 56 (1996) 222–241.
[3] H. Gao, Y. He, P. Shen, J. Zou, N. Ku, Y. Jiang, B. Huang, C.T. Liu, Intermetallics 17 (2009) 1041–1046.
[4] C. Wei-Jen, C.-J. Wang, Surface and Coating Technology 204 (2009) 824–828.
[5] K. Karczewski, S. Jóźwiak, Z. Bojar, Inżynieria Materiałowa Nr 3–4 (2007), s. 7 (552-228).
[6] R. Pampuch, Solid State Ionics 101–103 (1997) 899–907.
[7] S. Dong, P. Hou, H. Yang, G. Zou, Intermetallics 10 (2002) 217–223.
[8] U. Anselmi-Tamburini, G. Spinolo, G. Flor, Z.A. Munir, Journal of Alloys and Compounds 247 (1997) 190–194.
[9] S. Jóźwiak, K. Karczewski, Z. Bojar, International Journal of Powder Metallurgy 3 (4) (2009) 40–44.
[10] S. Jóźwiak, K. Karczewski, E. Pocheć, Z. Bojar, European Congress on Advanced Materials and Processes, Euromat 2009, 7–10 September, Glasgow, United Kingdom, 2009.
[11] A.A. Abu-Sehly, S.N. Alamri, A.A. Joraid, Journal of Alloys and Compounds 476 (2009) 341–348.
[12] F. Liu, G.C. Yang, J.N. Ciu, Termochimica Acta 438 (2005) 83–89.
[13] G. Ruitenberg, E. Woldt, S.A.K. Petford-Long, Termochimica Acta 378 (2001) 97–105.
[14] P. Supaphol, Termochimica Acta 370 (2001) 37–48.
[15] T.B. Masalski, American Society for Metals, Metals Park, Vol1, 1986, p. 112.
[16] J.M. Hey, D.R. MacFarlane, Journal of Non-Crystalline Solids 211 (1997) 262–270.